

# Chapter 5

## Time expansion chambers analysis

### 5.1 Introduction

Section 3.3 described time expansion chambers (TECs) that measure the trajectories of individual muons. This chapter will describe the analysis steps that convert the signals from the electronics to a position and angle; these are outlined in Fig. 5.1. This analysis is almost independent of the DCs and PCs. The TECs are in a region of weak magnetic field, so that trajectories are well approximated by straight lines. Complications arise due to electronics noise, crosstalk, sparks, beam positrons, multiple muons and inefficiencies.

The author undertook an extensive review of the existing code, making improvements, testing robustness, and documenting the algorithm. The straight line fitting method has not been described in detail elsewhere. Since the TECs are essential to  $P_\mu^\pi \xi$ , an entire chapter is reserved to describe their analysis and performance. The chapter will occasionally mention polarisation changes. Be aware that a change of  $1 \times 10^{-4}$  is negligible.

Note that throughout this chapter a “hit” is defined to be a distinct signal pulse.

### 5.2 Beam profiles

The reconstructed muon trajectories are used to create an input beam for the simulation. This is described in the simulation chapter, in Section 6.5. For the current chapter, a qualitative appreciation of the muon beam is necessary, since robustness tests used real TEC data. Figure 5.2 shows the characteristics of a nominal beam profile: the average position is approximately  $(0, 0)$  cm, with an average angle of  $\approx 0$  mr with respect to  $x$  and  $y$ . In the  $x$ -plane the beam is slightly divergent, and in the  $y$ -plane the beam is convergent. The figure shows two profiles that result in larger depolarisation; one profile is steered to have an average angle of  $\theta_y \approx 30$  mr, and the other profile is steered in  $x$  and  $\theta_x$ . The robustness of these profiles provide a more severe test of the TEC analysis code.

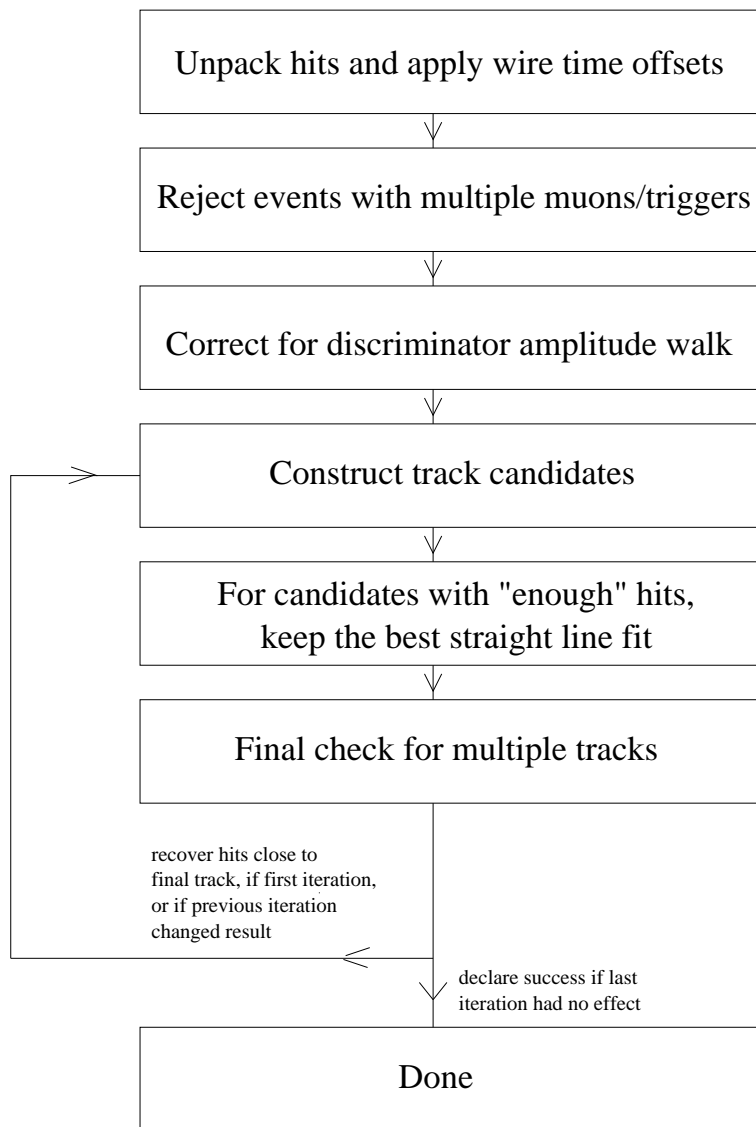
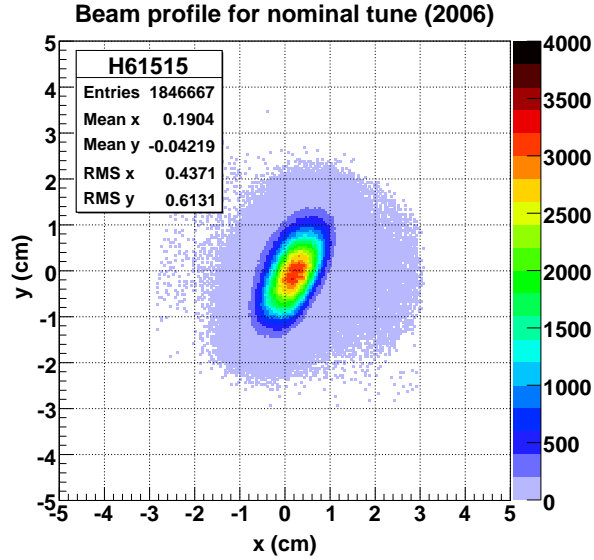


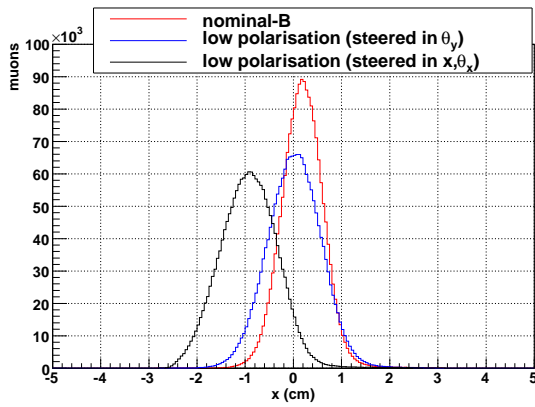
Figure 5.1: Flowchart of the steps in the TEC analysis.

### 5.3 Typical raw events

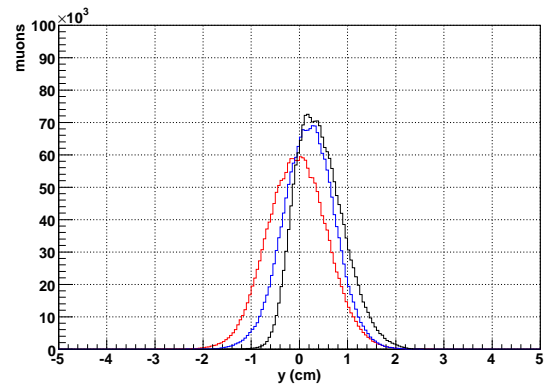
A selection of events from real data are shown in Fig. 5.4. The majority of events are like Fig. 5.3(a), with a single clean track through both modules, with most of the wires producing a signal. Some of the wires have multiple hits due to the break-up of ionisation into clusters and cross-talk, and this prevents a simple straight line fit from being applied to each hit's leading edge. Figures 5.3(b) and 5.3(c) show examples of the noise that must be separated from the genuine track. The noise in Fig. 5.3(b) only affected seven of the wires in the  $x$ -module. An example of two clean multiple muon tracks is shown in Fig. 5.3(d). The events



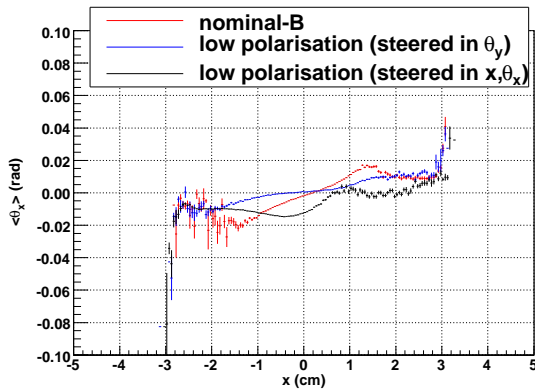
(a) Beamspot for nominal-B.



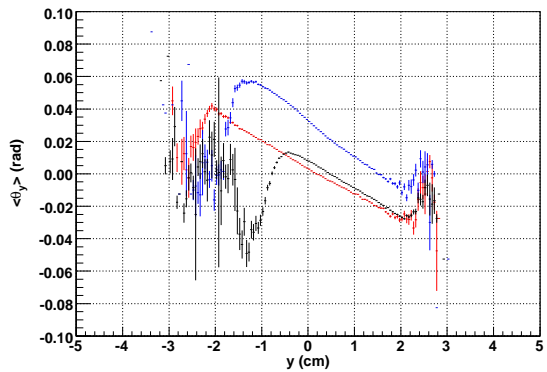
(b)  $x$ -projections.



(c)  $y$ -projections.



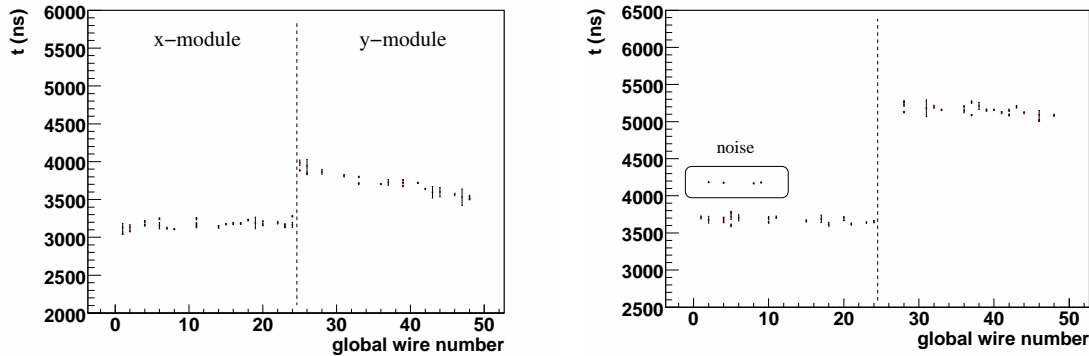
(d)  $\theta_x$ - $x$  correlation.



(e)  $\theta_y$ - $y$  correlation.

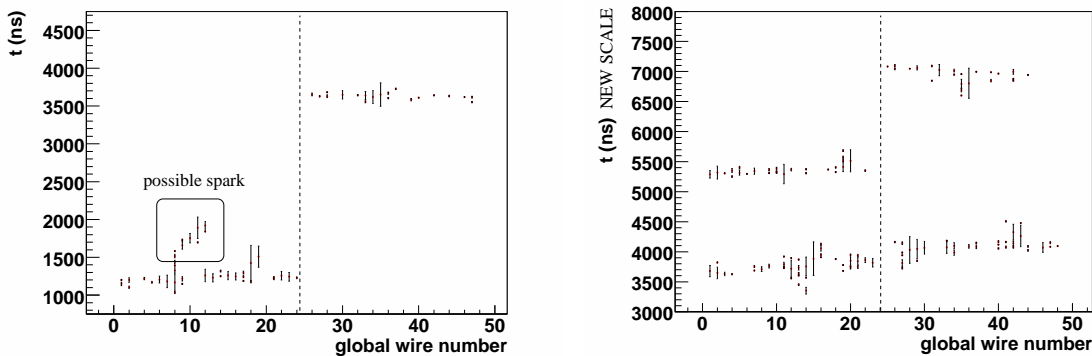
Figure 5.2: Beam profiles used to test the robustness of the TEC analysis code.

shown in Fig. 5.4 are all from data where the single wire efficiency was high. In practice, the sense planes aged over a period of hours, and the single wire efficiency reduced. This aging will later be treated as a systematic uncertainty.



(a) Clean event.

(b) Event with noise in x-module.



(c) Event with possible spark.

(d) Multiple muon event. Note the change in scale.

Figure 5.3: Examples of real TEC events. Wires 1 to 24 are the  $x$ -module, and 25 to 48 are the  $y$ -module.

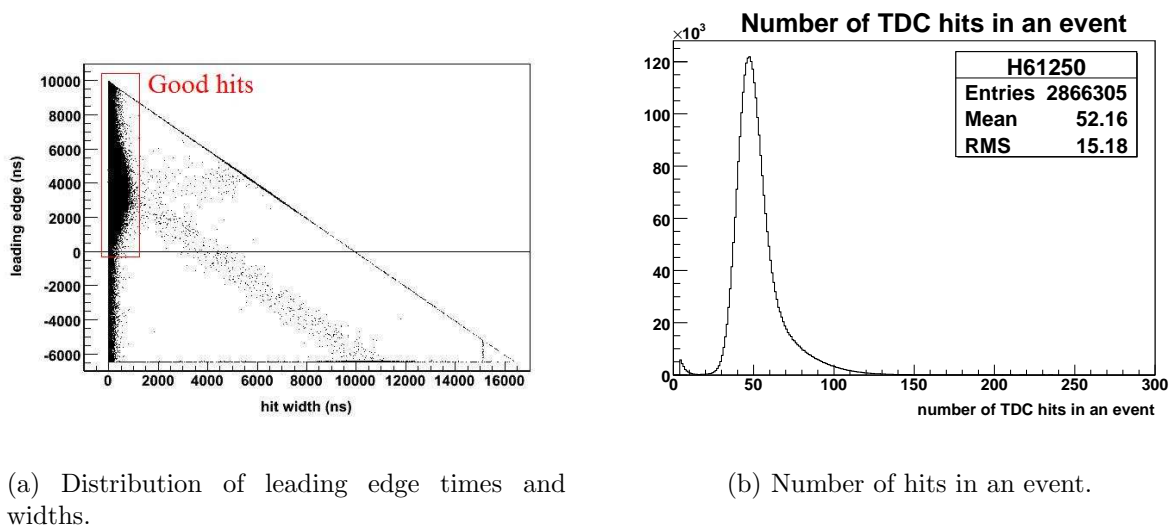
## 5.4 Analysis

### 5.4.1 Unpacking and wire time offsets

An event was analysed if it contained a muon separated by more than 700 ns from another particle. This corresponded to  $\approx 80\%$  of events, although including the other 20% was found to introduce no measurable bias. The trigger particle also had to pass the time of flight selection described in Section 4.3.2. The leading edge times and hit widths are shown in Fig.

5.4(a), where good hits (i.e. those unpacked properly by the TDCs to have a leading and trailing edge) are indicated. An improvement for the current analysis was to remove bad hits, as determined by an error code from the TDC. This increased the number of reconstructed tracks by a small amount ( $< 0.1\%$ ), but the beam profiles were negligibly changed.

The number of total hits in an event ( $x$ -module plus  $y$ -module) is shown in Fig. 5.4(b). If an event had less than four hits it was rejected, although the figure suggests the cut could be raised to  $\approx 20$  hits. This was investigated, and found to make no difference since events with  $< 20$  hits mostly corresponded to beam positrons that were already eliminated by later cuts.



(a) Distribution of leading edge times and widths.

(b) Number of hits in an event.

Figure 5.4: Raw hits for the TEC analysis.

The single wire efficiency, which was found to be independent of the beam tune, is shown in Fig. 5.5. A single wire does not fire for about one third of events, which is a lower efficiency than the original design specification. This efficiency reduced as the TEC planes aged. For the current analysis, the planes were changed on a regular basis to ensure that inefficiency did not introduce a significant systematic uncertainty.

## 5.4.2 Reject multiple trigger events

Events with multiple muons must be rejected, since they produce two tracks in each TEC module that cannot be matched up between the modules (see Fig. 5.3(d)). If the classification from Section 4.2.4 identifies two muons in the event, then it is removed at this stage in the

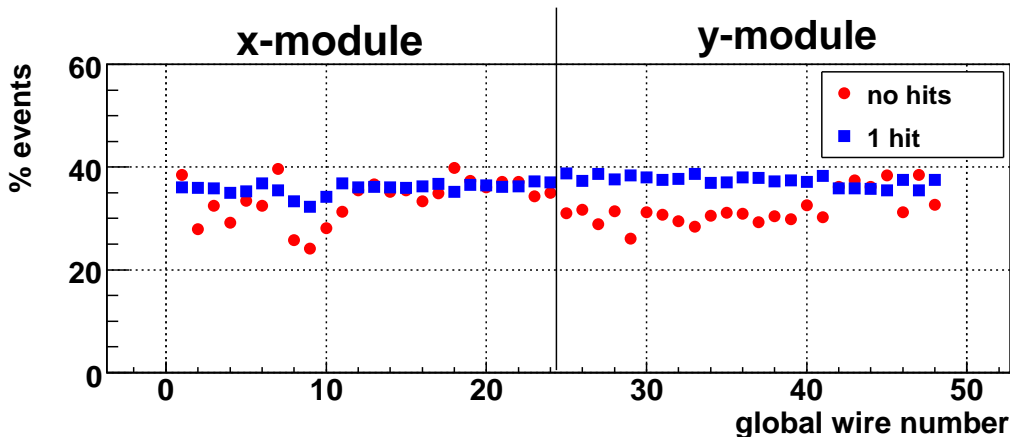


Figure 5.5: The single wire efficiency for a nominal tune is shown. For approximately  $\frac{1}{3}$  of events, an individual wire will not register a hit.

TEC analysis. This is the only place where information from inside the detector is used. The number of scintillator hits is also available, but not used if an event classification is available. Tests were carried out with no multiple muon removal, a cut on only the number of scintillator hits, and a cut on both the event classification and scintillator hits. The number of reconstructed muon tracks changed, but the effect on the beam profiles was negligible and the largest change in predicted polarisation was  $1 \times 10^{-4}$ .

At the end of the analysis chain there is another check for multiple tracks. See Section 5.4.7.

### 5.4.3 Hit width cut

The flowchart in Fig. 5.1 does not include a cut on pulse width. Such a cut was investigated in detail, since crosstalk and noise have short widths. Making a cut is not straightforward since good hits also have short widths, and there is expected to be a dependence of width on muon angle, since it's related to energy loss.

The distribution of hit widths for wire-1 is shown in Fig. 5.6. There is a peak around  $\approx 9$  ns that is more prominent for the  $x$ -module wires prone to the noise in Fig. 5.3(b). The majority of hits have widths around 18 ns, and ionisation clusters can merge together to create the tail of larger widths. The mean pulse widths on each wire are only consistent if hits below 20 ns are eliminated.

Removing widths of less than 10 ns increased the number of reconstructed tracks by between 2% and 5%, and had no impact on the position/angle distributions, or the polarisation.

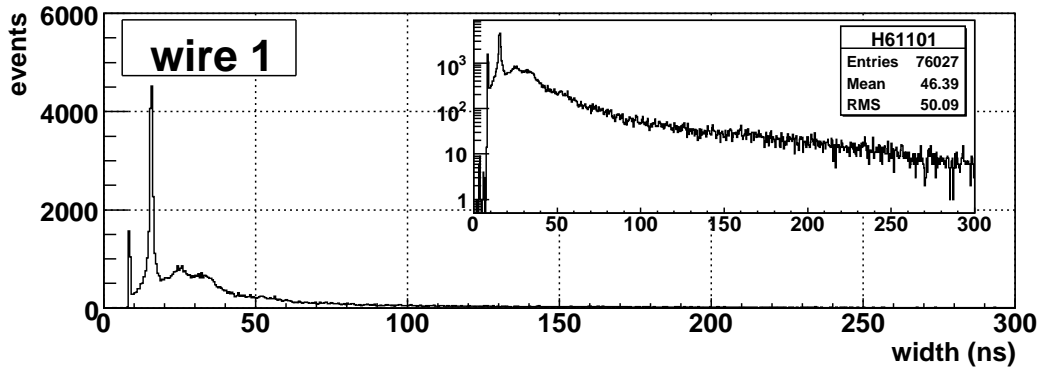


Figure 5.6: Distribution of hit widths for wire-1.

Removing widths of less than 20 ns degraded the polarisation by up to  $10 \times 10^{-4}$  due to an increase in the RMS of reconstructed angles (for example, the RMS of  $\theta_x$  for a nominal beam profile increased from 14.0 mr to 15.6 mr). The RMS increases because there are good hits with widths down to  $\approx 8$  ns, and removing these makes an individual angle less well determined. Figure 5.7 shows this, since hits of width  $< 10$  ns (green triangles) exist both in the noise around 1.4 cm, and on the real track.

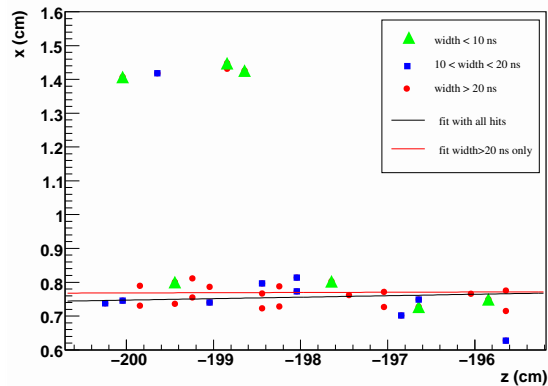
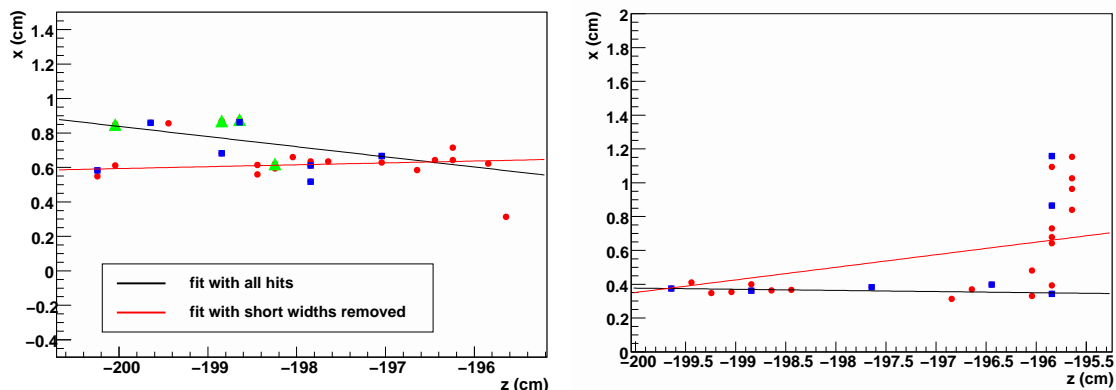


Figure 5.7: Event that demonstrates good hits can have short widths.

Figures 5.8(a) is an example where excluding short width hits can improve the angle measurement, and Fig. 5.8(b) is an example of where it degrades the angle measurement. Since the net effect of removing short width hits was equivalent to reducing efficiency, the final analysis did not include a cut on pulse width. Instead the pattern recognition was improved to better remove noise.



(a) Event where reconstructed angle is *improved* (and changes by more than 50 mr) when widths  $t < 20$  ns are excluded.

(b) Event where reconstructed angle is *worse* (and changes by more than 50 mr) when widths  $t < 20$  ns are excluded.

Figure 5.8: Event displays for width cut discussion. The displays do *not* have a common vertical scale.

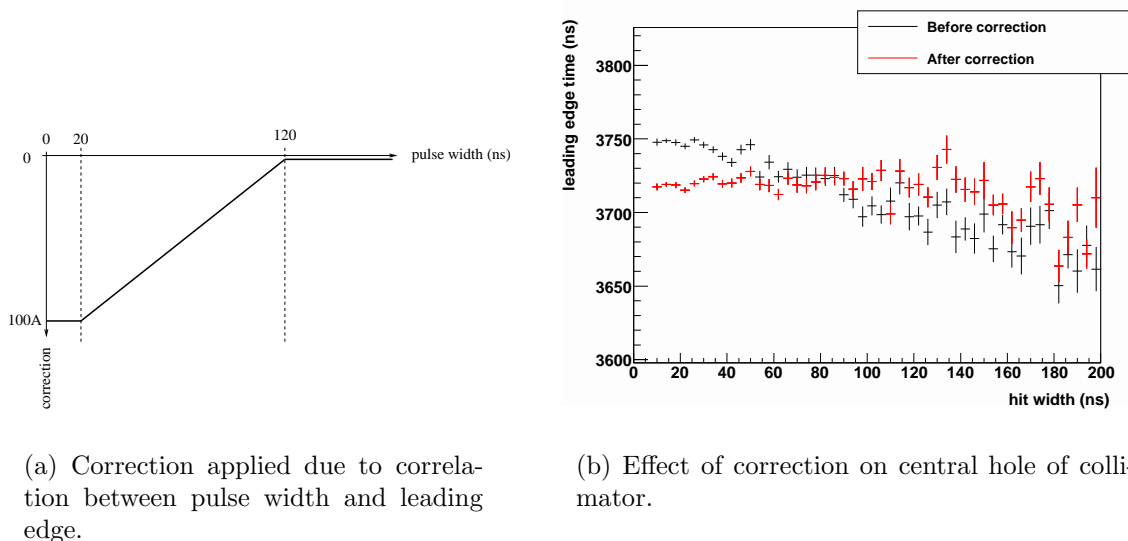
#### 5.4.4 Discriminator discriminator walk

Section 3.16 described the concept of discriminator amplitude walk, where the leading edge time is seen to have a correlation with hit width. At this step in the analysis, the leading edge times are corrected according to their width. The width-dependent correction is shown in Fig. 5.9(a), where  $A$  is calibrated for each wire. The effect on the leading edge times of muons passing through the central hole of the collimator (see Fig. 3.26(a)) is shown in Fig. 5.9(b), where the correction is as large as 50 ns for short widths. A test was carried out with the correction disabled, and the nominal profile changed negligibly, while the low polarisation profiles altered so that  $P_\mu$  changed by  $1 \times 10^{-4}$ . In the previous analysis the discriminator amplitude walk had more effect, since the calibration was not iterated until convergence (typically three iterations).

#### 5.4.5 Construct track candidates

Track candidates were constructed according to the algorithm in Fig. 5.10, which has the following steps:

1. Select a single hit.
2. Draw a corridor  $\pm 350$  ns from this hit.



(a) Correction applied due to correlation between pulse width and leading edge.

(b) Effect of correction on central hole of collimator.

Figure 5.9: Figures to demonstrate correction for discriminator amplitude walk.

3. On each wire, pick up the single hit that is within the corridor, and closest to the hit in (1).
4. If there are more than four hits, then keep this selection as a track candidate.
5. Repeat (1) to (4) for every hit.

This algorithm gives every hit a chance of being a good hit, and only allows one hit per wire. There is a small bias towards low angles since only the closest hit in time is selected.

The fixed corridor of  $\pm 350$  ns was investigated. In the simulation, removing the corridor altogether had a negligible effect on the muon reconstruction. The corridor only exists to allow the pattern recognition to work on data, where beam positrons and noise add complexity. In the nominal case, reducing (increasing) the corridor time to  $\pm 175$  ns ( $\pm 700$  ns) changed the RMS of  $\theta_x$  from 14.0 mr to 12.0 mr (17.0 mr), which is a significant effect. A corridor that is too narrow will have a strong bias towards low angles (Fig. 5.11(a)), and a corridor that is too large is susceptible to making track candidates with noise hits (Fig. 5.11(b)). There are at least two approaches to making the algorithm robust to corridor size; firstly the corridor can be made large, and hits rejected if they are too far from adjacent hits. Secondly the corridor can be kept small, and the initial fit treated as a guess to the true trajectory; hits are then recovered within a reasonable distance of the guess, and the process iterated until convergence. The first approach was found to be biased towards low angles, and therefore

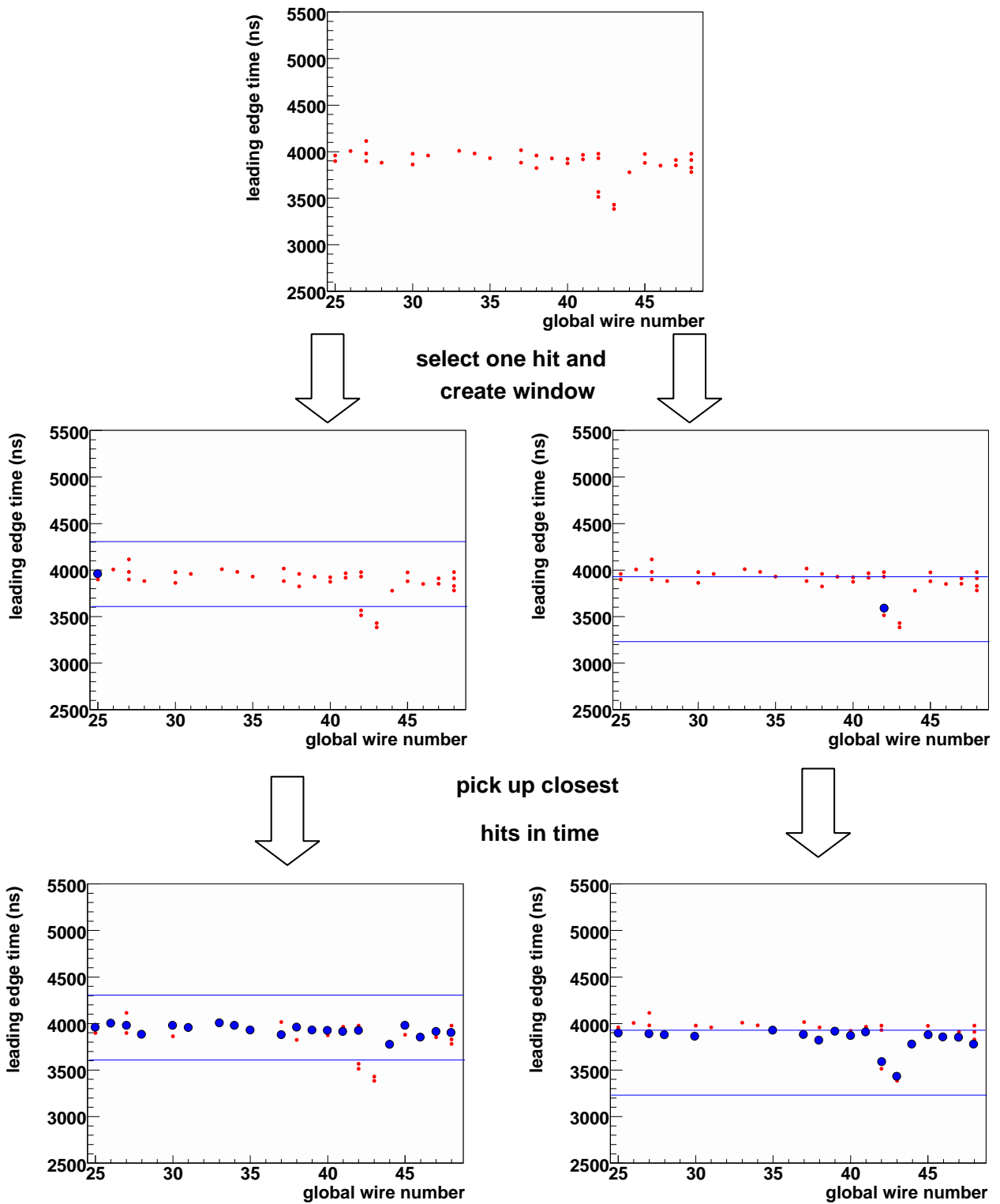
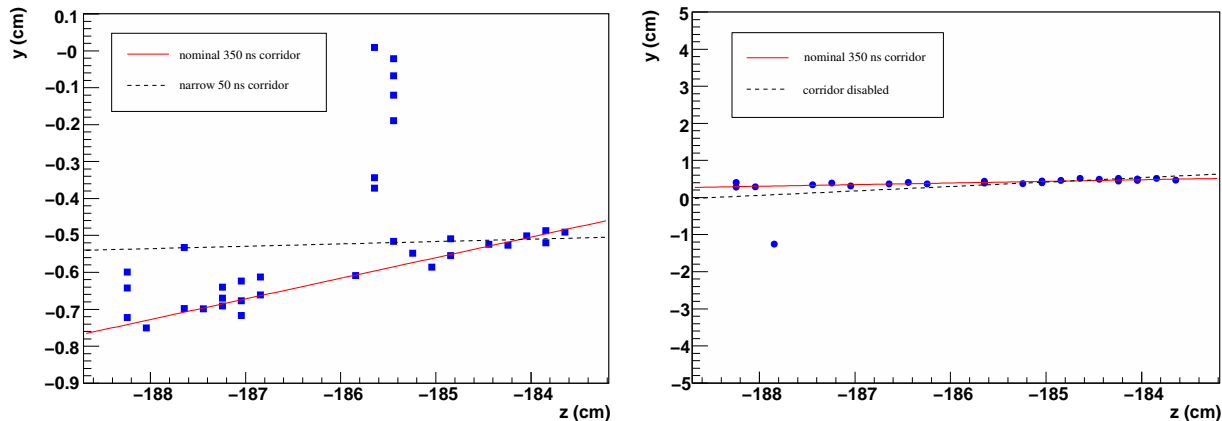


Figure 5.10: Demonstration of the construction of two possible track candidates. See the text for details on each step.

rejected. The second approach was implemented, and its tuning is described later in Section 5.4.8.



(a) A narrow corridor has a bias towards low angles.

(b) A large corridor is susceptible to noise.

Figure 5.11: Demonstration of problems from setting the corridor size too narrowly and too widely.

For the current analysis, the span of hits was also calculated for each track candidate. This is the difference in  $z$  between the first and last point on the track candidate. For a smaller span the angle is less well determined, and track candidates were only kept if their span was  $\geq 2.7$  cm ( $\geq 14$  out of 24 wires). In previous analyses this span was only calculated and used as a selection for the successful track. The tuning of the span and the choice of corridor size are closely related, and are discussed together in Section 5.4.8.

From this point onwards, the hits are managed in the track candidates.

### 5.4.6 Fit the track candidates with “enough” hits

The track candidate with the most number of hits ( $n_{\max}$ ) is found. The other track candidates are kept only if they met the following criteria:

- For  $n_{\max} > 12$ , require  $n \geq (n_{\max} - 2)$
- For  $8 < n_{\max} \leq 12$ , require  $n \geq (n_{\max} - 1)$ .
- For  $n_{\max} \leq 8$ , require  $n = n_{\max}$ .

Disabling the selection degrades the polarisation by  $8 \times 10^{-4}$  for all the profiles. This is because the TEC analysis code will tend to pick junk tracks such as the “spark” in Fig. 5.3(c). Therefore the selection was kept for the current analysis.

The leading edge times in the track candidates are then converted to distance, using an STR described by a cubic function,

$$s = p_0 + p_1t + p_2t^2 + p_3t^3, \quad (5.1)$$

where  $s$  is  $x$  or  $y$ , depending on the module, and  $p_i$  are determined by the calibration technique described in Section 3.16. A least-squares straight line fit is then carried out to the positions, and the track candidate with the smallest residuals is the successful muon trajectory.

### 5.4.7 Final multiple track removal

Even though events with two muons are reliably removed using the earlier event classification cut, there is still the possibility of multiple tracks due to noise and sparks (see Figs. 5.3(b) and 5.3(c)), and beam positrons, which are detected with low efficiency. In a module, if the best-fit track and another track candidate with enough hits (as determined in Section 5.4.6) are too close, the event is rejected.

The separation time was tuned for the current analysis. The old value of  $1 \mu\text{s}$  was conservatively large, and a setting of  $0.3 \mu\text{s}$  was found to be better at rejecting multiple track events, or those confused by noise. This change had a negligible effect on average positions and angles, and changed the RMS of reconstructed angles by  $< 0.6 \text{ mr}$ .

### 5.4.8 Iterating the algorithm

Section 5.4.5 described the construction of track candidates using a corridor time and the span of the hits in  $z$ . An iterative algorithm was described, where an initial fit is carried out using a narrow corridor, and hits are then recovered within a fixed distance, and the process iterated until convergence. This approach required the tuning of three parameters: the half corridor size, the span in  $z$  (“z-span”), and the distance over which hits should be recovered at each iteration (the “recovery distance”).

There is a minimum  $z$ -span requirement of approximately 2.7 cm to effectively remove noise from the data. There is also a maximum angle of approximately 200 mr; anything larger has a very low probability of triggering the muon scintillator that acts as the experiment’s trigger. These led to a constraint on the total corridor size of  $2.7 \text{ cm} \times \tan(0.2) \approx 0.55 \text{ cm} \approx 550 \text{ ns}$ , or a minimum *half* corridor size of  $\pm 275 \text{ ns}$ .

The corridor size and recovery distance were tuned by trying combinations of half corridor size in the range 100 ns to 700 ns, with recovery distances of 0.05 cm, 0.1 cm, 0.2 cm and 0.3 cm. The average positions and angles for the profiles were insensitive, except for the low polarisation set with  $\theta_y \approx 28$  mr, which is shown in Fig. 5.12(a). The only sensitive RMS was  $\theta_y$ , which is shown for a low polarisation set in Fig. 5.12(b); the  $\theta_y$ -RMS for the other profiles have similar behaviour. For the final analysis, a half corridor time of 300 ns was used, with a recovery distance of 0.15 cm. Only about 15% of events required a third iteration. Real data event displays were examined, but it wasn't clear whether iterating offers a definite improvement. If the difference in angle-RMS between the algorithms (3 or 4 mr) is larger than uncertainties in the correction for multiple scattering (see Section 6.2), it should be included as a systematic uncertainty.

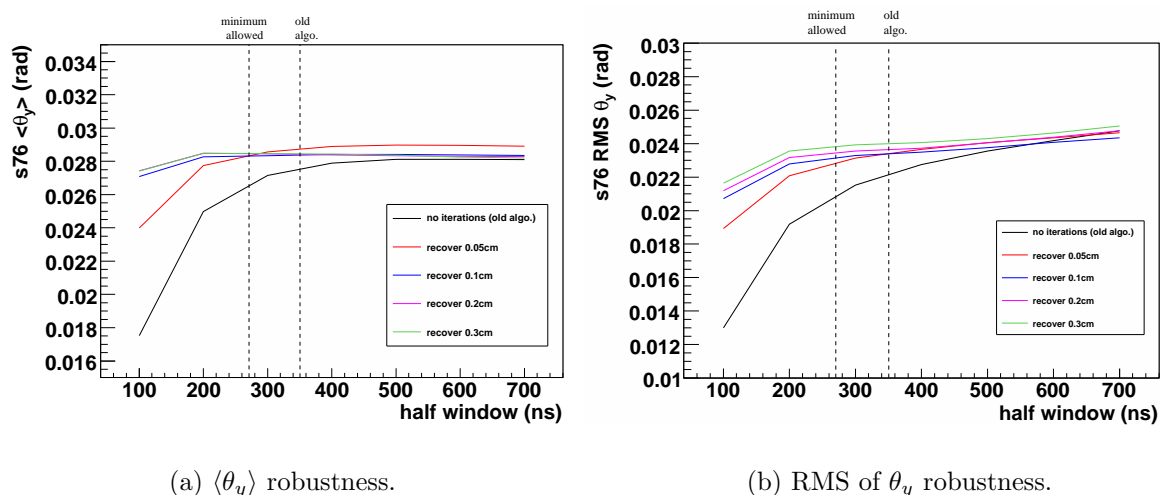


Figure 5.12: Robustness of  $\langle\theta_y\rangle$  and RMS of  $\theta_y$  to algorithm.

### 5.4.9 Other algorithms

Alternative reconstruction algorithms were tested, such as a Hough Transform, Kalman filter and iterative straight line fitting with outliers rejected at each stage. However they were found to need careful tuning to become robust to the noise in the data, and could not readily determine the RMS of angles better than the algorithm described in this chapter.

## 5.5 Performance

### 5.5.1 Resolution

The single hit resolution for each wire was determined as follows:

1. For the track candidate with lowest  $\chi^2$ , re-fit with a wire excluded.
2. For the excluded wire, histogram the residual distance between the hit and the fit.
3. Find the RMS of the residual histogram. This is a measure of the single hit resolution for the wire.

The results are shown in Fig. 5.13, where the resolution is between  $275\ \mu\text{m}$  and  $375\ \mu\text{m}$  for all wires, and is seen to worsen at the edges of the modules where the field has the largest non-uniformities. The resolution degrades as the planes age, but not by a significant amount. The single hit resolution also depends on the distance from the sense plane, and is as low as  $150\ \mu\text{m}$  close to the sense plane[30].

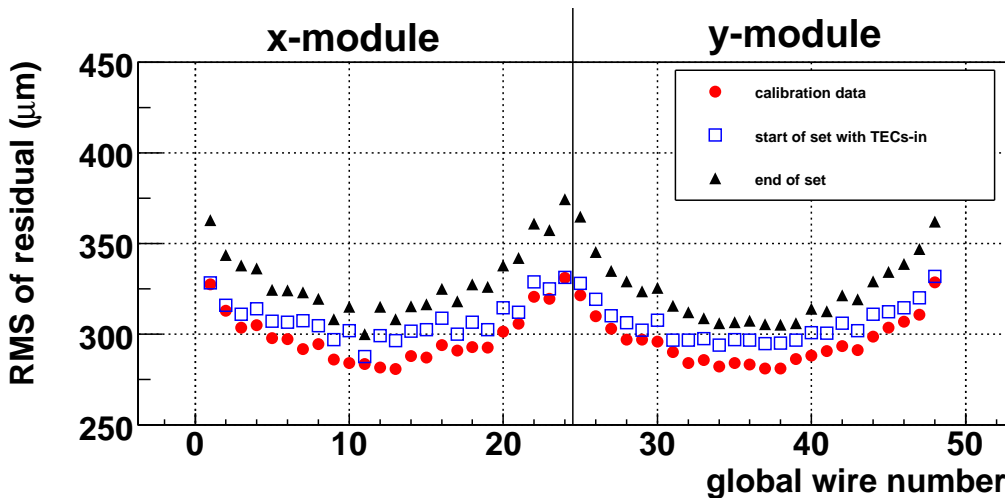
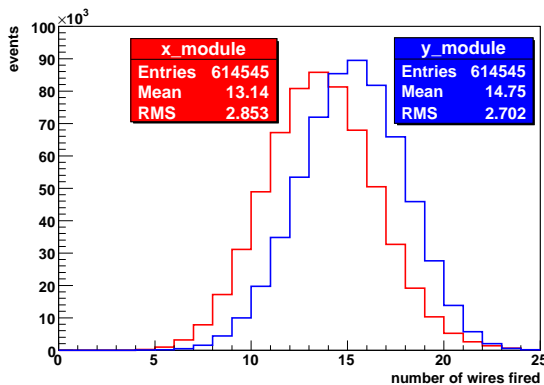


Figure 5.13: Resolution (RMS of residual distribution, when wire is excluded from fit).

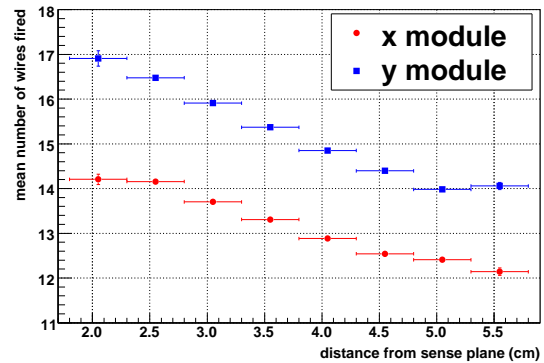
The resolution of the track position and angle can be determined using simulation. With wire inefficiency simulated, and no multiple scattering, the track angle resolution is  $\sim 3\ \text{mr}$ , and the track position resolution is  $\sim 150\ \mu\text{m}$ [36]. However, this is misleading since the track resolution in the data will be lower due to the noise.

## 5.5.2 Position dependent efficiency

The number of wires fired per event is shown in Fig. 5.14(a). As an ionisation cluster drifts, its electrons separate in time. Therefore a longer drift time will result in a lower probability of a hit exceeding the electronics threshold. This is visible as a reduction in the number of wires fired per event with distance, as shown in Fig. 5.14(b). The number of wires fired is still high, even far from the sense plane, and there are no observed asymmetries in the beam profile.



(a) Number of wires fired.



(b) Distant-dependent efficiency.

Figure 5.14: Number of wires fired in a real characterisation run.

## 5.6 Calibration and alignment

The calibration techniques were briefly described in Section 3.16. The current section will compare the results from the four independent calibrations in 2006 and 2007. Note the final calibration was carried out after the analysis code was finalised.

### 5.6.1 Wire time offsets

The wire time offsets are compared in Fig. 5.15. Recall these are determined by placing 121 hole collimators on both ends of the box containing the TECs, and selecting tracks that pass through the central hole (diameter 0.1 cm). There is a clear systematic slope that

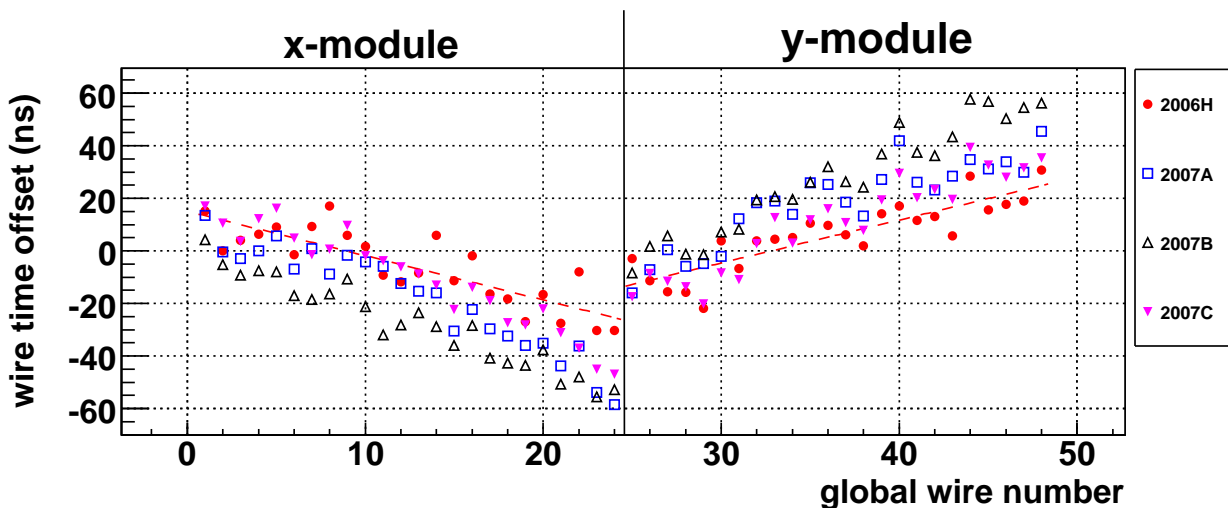


Figure 5.15: Comparison of wire time offsets for the calibrations in 2006 and 2007. The gradient corresponds to a rotation of the TECs within their box of between 7 – 12 mr. A fit line is included for 2006H only.

corresponds to a rotation of 7 – 12 mr in each module<sup>39</sup>. The collimators are aligned to better than  $500\ \mu\text{m}$ , which corresponds to 3 mr over their separation distance (16 cm); therefore the wire time offset calibration must be aligning the individual TEC modules within their box, not correcting for a misalignment of the collimators. The previous analysis found similar features that suggested a 2 – 4 mr rotation, but the statistical precision was significantly worse.

The possible time variation over a 0.1 cm diameter hole is  $< 1\ \text{ns}$ , so that the remaining features in Fig. 5.15 are differences in cable lengths and electronics.

### 5.6.2 Discriminator amplitude walk

The  $A$  parameters, as defined in Fig. 5.9(a), are compared for each wire in Fig. 5.16. There is no clear evidence of wire-to-wire differences, which if they existed would indicate a difference in electronics thresholds. The parameters are remarkably consistent between calibrations.

<sup>39</sup>The gradient for the 2006H planes is between  $-1.7\ \text{ns}$  and  $-2.6\ \text{ns}$  per wire in the  $x$ -module, and between  $1.6\ \text{ns}$  and  $2.8\ \text{ns}$  per wire in the  $y$ -module.  $1\ \text{ns}$  is approximately  $9\ \mu\text{m}$ , and the wires are 0.2 cm apart, so that the rotation is 8 – 11 mr in the  $x$ -module, and 7 – 12 mr in the  $y$ -module.

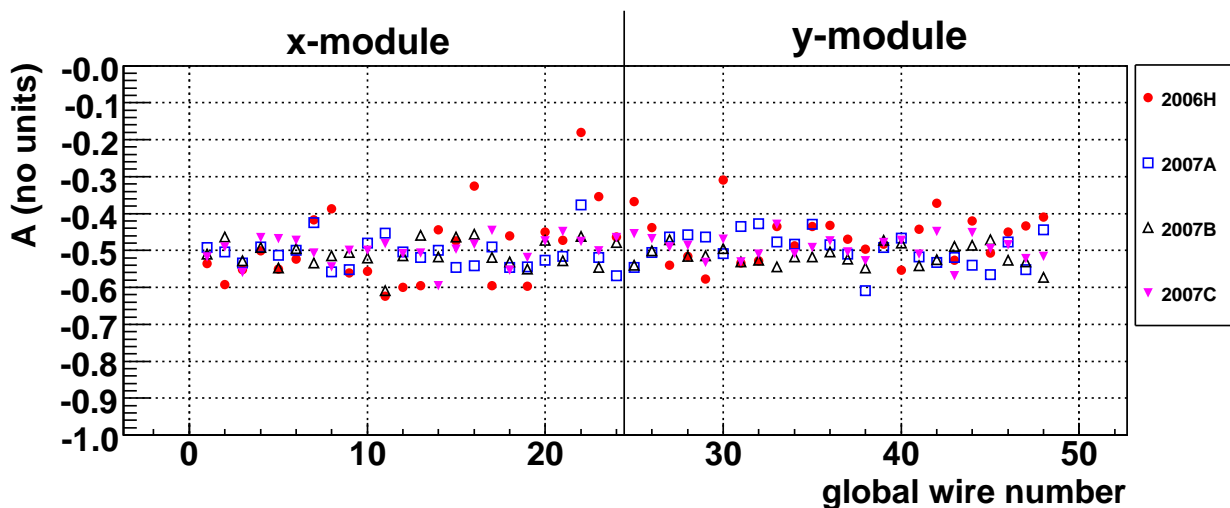


Figure 5.16: Comparison of amplitude discriminator walk parameters for the calibrations in 2006 and 2007. The correction is measured to be independent of wire and sense planes, as it should be.

### 5.6.3 Space-time relationship

A comparison of the space-time relationships (STRs) for wire 12 in the  $x$ -module is shown in Fig. 5.17, including the effect of a temperature correction<sup>40</sup>. This calibration corrects for plane and wire misalignments, electric field distortion and field penetration between the modules. After correcting for temperature the calibrations are very consistent.

The importance of temperature correcting the STRs was considered. A change of  $\pm 3^\circ\text{C}$  altered the mean positions by  $< 500 \mu\text{m}$ , and the mean angles by  $< 0.4 \text{ mr}$ , which are already negligible amounts. Figure 5.18 shows the temperatures of TEC measurements compared to the temperatures at which the STRs were calibrated. Since there is always a TEC measurement within  $1.5^\circ\text{C}$  of the calibration temperature, no correction was necessary.

<sup>40</sup>The gas inside the TECs was held at a constant pressure, so that temperature variations altered the gas density and hence the space-time relationship. This was a linear effect that was easily corrected.

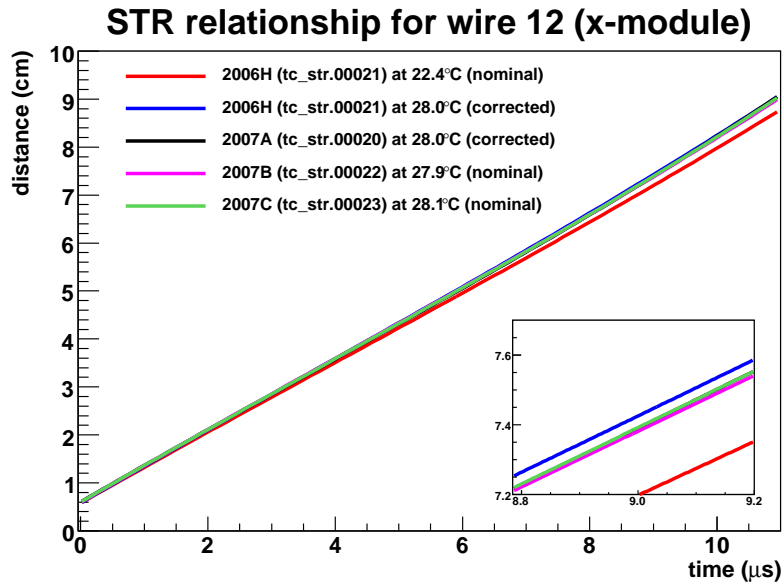


Figure 5.17: Comparison of space-time relationships for the calibrations in 2006 and 2007. After correcting for temperature differences, the STR is very consistent between different sense planes.

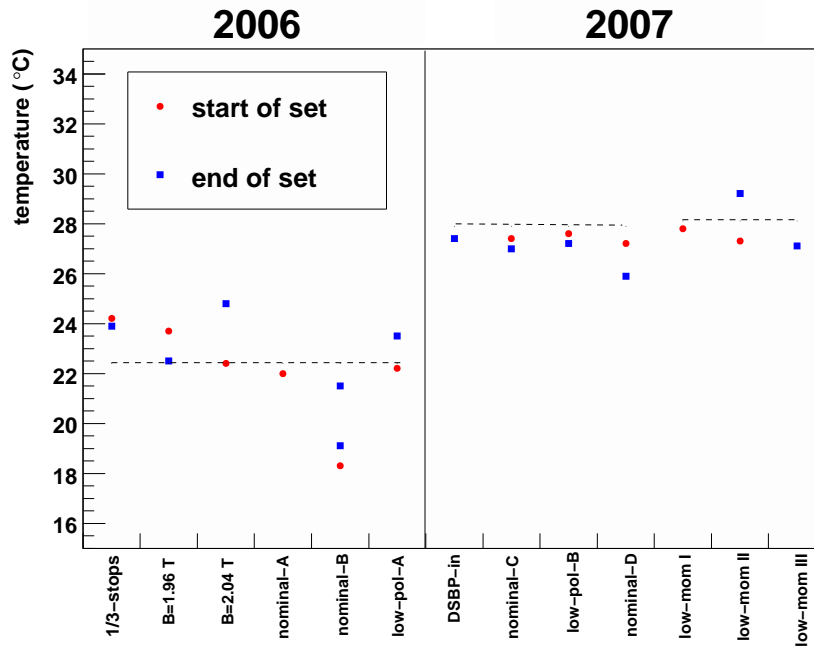
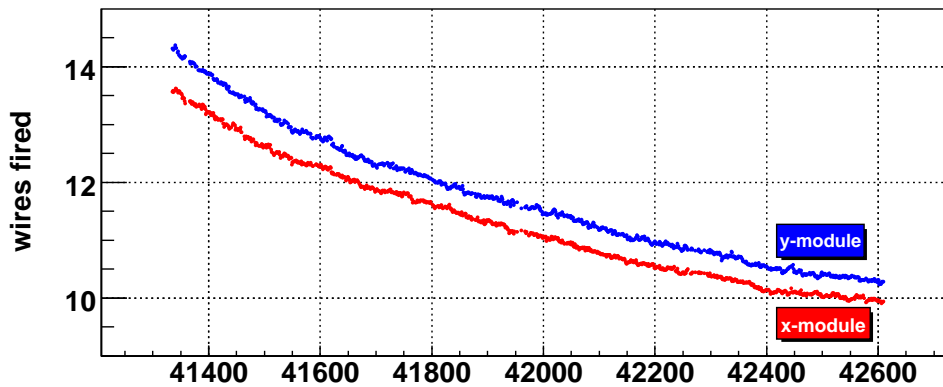


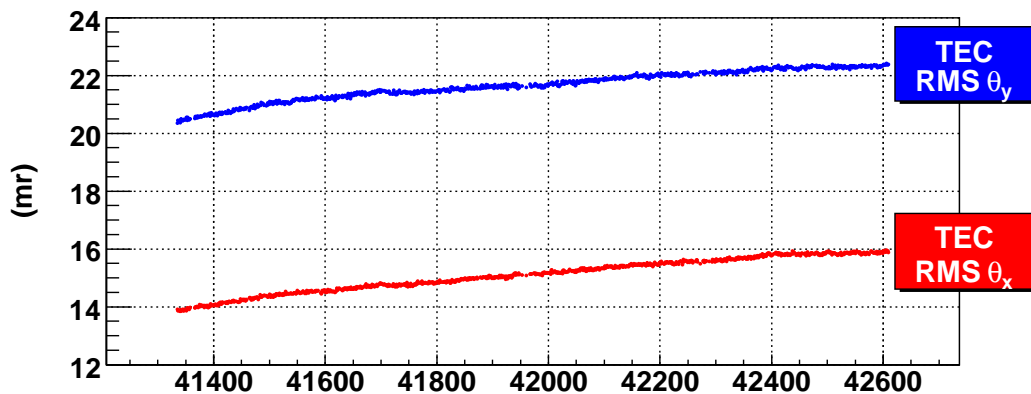
Figure 5.18: Comparison of TEC-data temperature and calibration temperatures. The dashed lines indicate the mean temperature for the calibration. For each data set, there is always TEC-data within 1.5°C of the calibration temperature.

## 5.7 Sense plane aging

An entire set was taken with a nominal beam tune and the TECs in place, allowing a study of the aging and muon beam stability. As will be seen in Section 8.5.8, the mean positions and angles were highly stable over the period of a week. However, as the sense planes aged, the number of wires fired per event decreased, which caused the angle to be less well determined and the RMS of reconstructed angles therefore increased. Figure 5.19 shows this effect, where the RMS is seen to change by 2 mr in each module, which corresponds to a change in polarisation of  $5 \times 10^{-4}$ . This information will be later used to assign a systematic uncertainty due to sense plane aging. There was also a negligible increase in the RMS of the positions over the entire set (0.04 cm).



(a) Number of wires fired in each module.



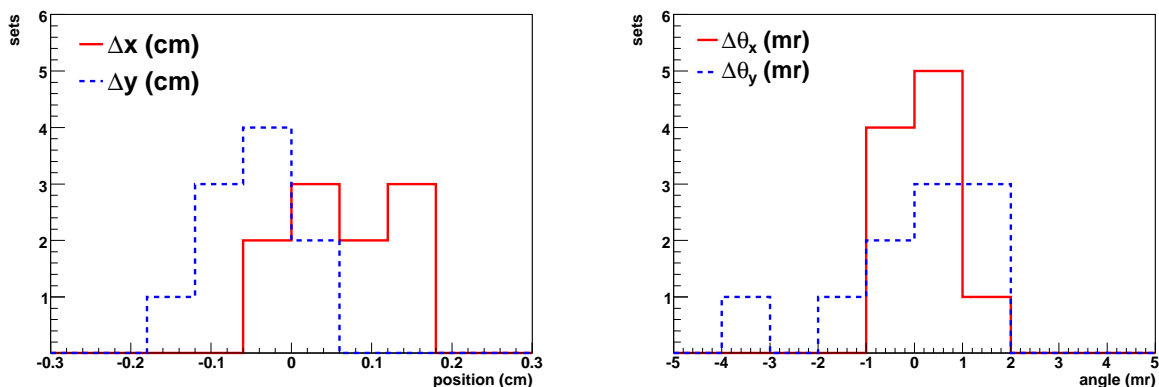
(b) RMS of reconstructed angles.

Figure 5.19: Sense plane aging. As the number of hits per event decreases, the angle is less well determined, and the RMS of reconstructed angles increases.

## 5.8 Reproducibility

The TECs were inserted at the start and end of most data sets, which typically lasted a week. The insertion/removal required the beam line elements to be switched off, and a breaking of the vacuum in the beam line, which then had to be pumped down again before the TECs could be used. The process exerted significant forces on the beam line components and box containing the TECs. An analysis of the muon beam chamber measurements suggested the beam was highly stable during sets, so that any difference in TEC measurements are due to their reproducibility in the insertion process.

The change in average position and angle are histogrammed in Fig. 5.20, where movements of up 0.2 cm were possible in position, and 4 mr in average angle. These discrepancies are much larger than the temperature differences, and dominate any of the uncertainties from alignments and analysis that have been described in this chapter. The difference in polarisation between these characterisation runs will be later used to estimate a systematic uncertainty.



(a) Change in average position.

(b) Change in average angle.

Figure 5.20: Histograms of the difference between the beginning and end of set characterisations. In total there are nine sets available.

## 5.9 Summary

The analysis code that reconstructs individual muon trajectories in the time expansion chambers has been described. The most significant uncertainty from the algorithm is an uncer-

tainty of 3 – 4 mr in the RMS of  $\theta_y$  due to the noise that exists in the data. The average angle is determined to better than  $< 1$  mr for the three profiles tested.

The performance of the TECs was documented. The single hit resolution is better than  $375 \mu\text{m}$  for all wires, and the available calibrations for wire time offsets, discriminator amplitude walk and space-time relationships are remarkably stable. There is an aging of the sense planes that must be included in a later systematic uncertainty. The dominant systematic uncertainty from the TECs is due to their reproducibility in position and angle.